Chapter 4
Laplacian Spectra and Synchronization Processes on Complex Networks

Juan Chen, Jun-an Lu, Choujun Zhan, and Guanrong Chen

Abstract The spectrum of the Laplacian matrix of a network contains a great deal of information about the network structure and plays a fundamental role in the dynamical behavior of the network. This chapter is to explore and analyze the Laplacian eigenvalue distributions of several typical network models, to study the network dynamics towards synchronization at a mesoscale level of description, and to report the finding of a relation between the spectral information of the Laplacian matrix and the dynamics in the network synchronization process. First, an example of adding long-distance edges is given to show that the network synchronizability may not be directly inferred from statistical properties of the network. Then, the Laplacian eigenvalues of several representative complex networks are shown to possess very different properties, and yet they also share some common features meanwhile. Further, the correlation between the Laplacian spectrum and the node-degree sequence of a network is investigated, revealing that scale-free networks have the highest correlation values, followed by random networks and then by small-world networks. To that end, a simple local prediction–correction algorithm is presented for approximating the eigenvalue λ_{i+1} from λ_i, $i = 1, 2, \cdots, N$, where N is the network size. Finally, it is shown that the processes of synchronization and generalized synchronization (GS) display different patterns, depending intrinsically on the topological structures of the networks. It is found that in the process of synchronization (or GS), roughly speaking, synchronization (or GS) first starts from a small part of hub nodes and then spreads to the other nodes with smaller degrees.

J. Chen • Jun-an Lu
School of Mathematics and Statistics, Wuhan University, Wuhan, Hubei 430072, China
e-mail: juanchen1220@yahoo.com.cn; jalu@whu.edu.cn

C. Zhan • G. Chen (✉)
Department of Electronic Engineering, City University of Hong Kong,
Hong Kong SAR, China
e-mail: zchoujun2@student.cityu.edu.hk; eegchen@cityu.edu.hk

It is also demonstrated that, for community networks, a typical synchronization process generally starts from partial synchronization through cluster synchronization to evolve to global complete synchronization.

4.1 Introduction

In recent years, the theory of complex networks has attracted wide attention and become an area of great interest [1–5], for its advances in the understanding of many natural and social systems. One subject in the studies of complex networks that has received a great deal of attention is the topological characterization of various networks. Indeed, there has been considerable interest in investigating how the statistical properties of a network, such as the degree distribution, average distance, clustering coefficient, betweenness, and so on, are related to the dynamical processes taking place on the network [6–14]. However, it was shown in [15] that some statistical network properties are not sufficient to determine various complex dynamical patterns. It is found that unfortunately statistical properties may actually infer completely opposite conclusions about some large-scale complex networks sometimes.

From a graph-theoretic perspective, the spectrum (i.e., the set of eigenvalues) of the Laplacian matrix of a network contains tremendous information about the underlying network, which provides useful insights into the intrinsic structural features of the network [16]. A prototype example is the synchronizability of a network [17–20], which is crucially determined by the ratio of the smallest nonzero eigenvalue to the largest one of the corresponding Laplacian matrix. Also, the eigenvectors of the Laplacian matrix are known to be useful for detecting the community structure of a network [21].

Synchronization, as an emerging phenomenon of a population of dynamically interacting units, has fascinated humans since the ancient times. Synchronization phenomena and processes are ubiquitous in nature and play a vital role within various contexts in biology, chemistry, ecology, sociology, technology, and even visual arts. To date, the problem of how the structural properties of a network influence the performance and stability of the fully synchronized states of the network have been extensively investigated and discussed, both numerically and theoretically. Regarding partial synchrony, however, research results obtained thus far are much less and unmature [22–32]. It is well known today that synchronization analysis, synchronization processes and topological scales are all crucially determined by the whole eigenvalues spectrum of the Laplacian matrix of the network [15, 24, 25]. As such, a careful investigation on the eigenvalues spectrum of a complex network is of great significance especially regarding the evolution of the dynamical behaviors of the network.

The present chapter studies the Laplacian spectra of complex networks and their effects on the synchronization processes over the networks. Specifically, it is to further explore and analyze the Laplacian eigenvalue distributions of several

typical network models, to study the network dynamics towards synchronization at a mesoscale level of description, and to report a connection between the spectra of the Laplacian matrix and the dynamical process through the emergence of network synchronization.

Section 4.2 introduces the notion of eigenvalues spectrum of the Laplacian matrix of a network, and some well-known estimations of the eigenvalues. As reported in [15], some networks with the same statistical properties may have very different synchronization characteristics. Here, in addition, an example is given to show that adding long-distance edges can sensitively affect the average distance, a typical statistical property, while the smallest nonzero eigenvalue remains essentially unchanged.

Section 4.3 introduces and analyzes the spectral distributions of regular, random, small-world, scale-free, and community networks. The main finding is that the Laplacian eigenvalues of these four types of complex networks have very different properties in general and yet they also share some common features meanwhile. The spectral distributions of regular, random, and small-world networks are homogeneous, whereas that of the scale-free networks is quite heterogeneous. Furthermore, for random and small-world networks, the smallest nonzero eigenvalue depends approximately linearly on the connection probability adopted in network generation. There exist some big gaps between consecutive eigenvalues in community networks, while for a network with k prominent communities there are $k - 1$ eigenvalues near zero. In various realizations of the same type of network topology of the same size, the variations of their Laplacian eigenvalues are quite small; and this is roughly the same for all different types of network models studied.

In Sect. 4.4, it is revealed that the distributions of the Laplacian eigenvalues are very similar to the distributions of the node-degree sequence. It is found that the correlation between the spectrum and the node-degree sequence of a scale-free network is the highest, followed by random networks and then by small-world networks. Meanwhile, a simple local prediction-correction algorithm is designed to determine the eigenvalue $\lambda_i + 1$ from λ_i, $i = 1, 2, ..., N$ where N is the size of the network. It is also demonstrated that the eigenvalue curves are quite different from their corresponding node-degree distributions in some regions with small indexes, although they are quite similar in other regions.

Section 4.5 studies the dynamics towards synchronization in complex networks at the mesoscale level of description. The dynamical processes towards synchronization show different patterns depending intrinsically on the network topological structures. It is found that the processes of synchronization and generalized synchronization (GS) display different patterns, depending intrinsically on the topological structures of the networks. It is also found that in the process of synchronization (or GS), roughly speaking, synchronization (or GS) first starts from a small part of hub nodes and then spreads to the other nodes with smaller degrees. Finally, it is demonstrated that, for community networks, a typical synchronization process generally starts from partial synchronization through cluster synchronization to global complete synchronization.

4.2 The Laplacian Matrix and Its Eigenvalues

Consider a network G of N nodes, with edges linking certain pairs of nodes together. Suppose that there are no self-loops and no multiple edges between the same pair of nodes. The Laplacian matrix L of the network is defined by

$$L_{uv} = \begin{cases} d_v & \text{if } u = v, \\ -1 & \text{if } u \text{ and } v \text{ are adjacent,} \\ 0 & \text{otherwise.} \end{cases}$$

where d_v denotes the degree of node v. The adjacency matrix $A = (a_{uv})$ is defined by $a_{uv} = 1$ if u is adjacent to v or 0 others. Thus, the Laplacian matrix L is defined to be $L = D - A$, where $D = (d_{ij})$ is the diagonal matrix of all node degrees, that is, with d_{ii} equals the degree of node i, $i = 1, 2, \ldots, N$. Only undirected networks are considered here, for which all the Laplacian matrices are symmetric and positive semi-definite, with nonnegative real eigenvalues arranged as $\lambda_1 \leq \lambda_2 \leq \cdots \leq \lambda_N$.

Since the Laplacian matrix, described as above, has zero row-sums (hence, zero column-sums), the smallest eigenvalue $\lambda_1 = 0$ with the corresponding eigenvector $(1, 1, \ldots, 1)^T$; in particular, λ_2 is nonzero if and only if the network is connected, and furthermore the number of connected components is equal to the multiplicity of the 0 eigenvalue.

4.2.1 Basic Properties of Laplacian Eigenvalues

Let $d_{\min}$ and $d_{\max}$ denote the smallest and the largest degree of a network, respectively, and use the index i to order the degrees of its nodes: $d_{\min} = d_1 \leq d_2 \leq \cdots \leq d_N = d_{\max}$. The following estimates are well-known [33]:

$$\lambda_2 \leq \frac{N}{N-1} d_{\min} \leq \frac{N}{N-1} d_{\max} \leq \lambda_N \leq 2 d_{\max}. \tag{4.1}$$

Similarly, using the average degree d_{avg}, it was shown in [34] that

$$d_{\text{avg}} < \lambda_N(A) \leq N, \tag{4.2}$$

where $\lambda_N(A)$ is the largest eigenvalue of the adjacency matrix A and, moreover, $\lambda_N(A) = N$ if and only if the complementary graph of G is disconnected [35]. However, the above estimations are generally conservative.

Fiedler [36] further established the following bounds relative to the node connectivity and the edge connectivity:

$$\lambda_2 \leq \upsilon(G) \leq e(G),$$

where $\upsilon(G)$ is the node connectivity of G, namely the minimal number of nodes whose removal together with the adjacent edges would result in losing the connectivity of G, while $e(G)$ is the edge connectivity, defined as the minimal number of edges whose removal would result in losing the connectivity of G.

Fiedler [36] also established a lower bound relative to the edge connectivity or to the largest degree, as follows:

$$\lambda_2 \geq 2e(G)(1 - \cos(\pi/N)),$$
$$\lambda_2 \geq 2[\cos(\pi/N) - \cos(2\pi/N)] - 2\cos(\pi/N)(1 - \cos(\pi/N))d_{\max}.$$

The second lower bound is better if and only if $2e(G) > d_{\max}$. Relatively, one also has $2(1 - \cos(\pi/N)) = \lambda_2(P_N)$, where $\lambda_2(P_N)$ the second smallest eigenvalue of the adjacent matrix corresponding to P_N, a path through N nodes.

Anderson and Morley [37] showed that

$$\lambda_N \leq \max\{d_u + d_v : u \text{ and } v \text{ are adjacent}\},$$

The equality holds if and only if G is a semi-regular bipartite graph.

Merris [38] showed that

$$\lambda_N \leq \max\{d_v + m_v\},$$

where m_v is the average degree of all the neighbors of node v.

Rojo, Soto, and Rojo [39] gave another upper bound on λ_N, as follows:

$$\lambda_N \leq \max\{d_u + d_v - |N_u \cap N_v| : u \neq v\},$$

where $|N_u \cap N_v|$ denotes the number of the common neighbors of nodes u and v.

Li and Pan [40] proved that

$$\lambda_{N-1} \geq d_{N-1},$$

where the equality holds for a complete bipartite graph or a tree with a degree sequence $\{N/2, N/2, 1, \ldots, 1\}$. Prior to this, it was known [41] that

$$\lambda_N \geq d_{\max} + 1,$$

where the equality holds if and only if $d_{\max} = N - 1$.

Last but not least, Duan, Liu, and Chen [42] reported some useful estimation bounds for some Laplacian eigenvalues and the eigenvalue ratio about complex network synchronizability, with respect to subgraphs, complementary and product graphs.

4.2.2 Statistical Properties Versus Laplacian Spectra

In [13], it was shown that the synchronizability of a large class of networks is determined by the eigenvalue ratio λ_2/λ_N, of which it was shown that the main dependence is on the smallest nonzero eigenvalue λ_2 [43, 44]. Since in most real networks, $d_{\min} = 1$, it follows from (4.1) that

$$\lambda_2 \leq N/(N-1),$$

which, of course, is a rather conservative estimation.

From (4.1), one immediately gets that

$$\frac{\lambda_2}{\lambda_N} \leq \frac{d_{\min}}{d_{\max}} \leq 1. \tag{4.3}$$

Therefore, generally speaking, the closer to 1 the ratio is, the better the network synchronizability will be. For example, that scale-free networks have $d_{\min}/d_{\max} \ll 1$; therefore, as has been well experienced, they have relatively poorer synchronizability in comparison to most other types of network structures in general.

It should be noted, however, that (4.3) does not imply that a more homogeneous degree distribution always means a better synchronizability. It was shown in [15] that the effect of small structural changes on synchronizability may not average out within a large-scale network, therefore the synchronizability may not be described by the statistical network properties. Moreover, some examples were presented in [15, 16] to show that networks with the same degree distribution can have very different synchronizability characteristics.

According to [15], furthermore, an upper bound of λ_2 can be estimated by

$$\lambda_2 \leq 2\frac{|\partial S|}{|S|}, \tag{4.4}$$

where S is any subset of nodes satisfying $0 < |S| \leq N/2$, $|S|$ is the total number of nodes in S, and $|\partial S|$ is the number of common edges between S and its complementary graph. It was also reported in [15] that the estimation (4.4) plays a key role in understanding why the statistical properties of a network may fail to determine λ_2. An important observation is that the above bound on λ_2 is determined by the properties of some subgraph S but not in general by the network itself. In particular, S can be very small comparing to the whole network, so in this case the statistical properties of the network need not be reflected by S, therefore the former may not be very crucial for bounding the value of λ_2.

Here, an example is given to further show that adding long-distance edges to a network can sensitively affect the average distance, but they have very little effect

a λ_2 and λ_2/λ_N versus probability p.

b λ_2 and λ_2/λ_N versus probability p.
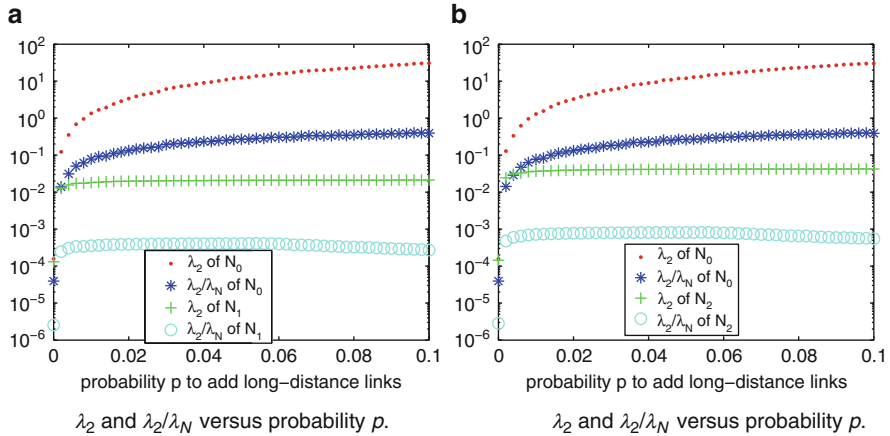
Fig. 4.1 Synchronizability comparison: (**a**) between network N_0, composing of a small-world model H of 500 nodes, and network N_1, composing of a small-world model H of 500 nodes and a fully connected model S of 50 nodes, with only one edge connecting H and S together; (**b**) between network N_0 and network N_2, composing of a small-world model H of 500 nodes and a fully connected model S of 50 nodes, with two edges connecting H and S together

on the smallest nonzero eigenvalue. To do so, consider a community network N_1 composing of a huge part H and a small part S, where H is a small-world model of 500 nodes and S is a fully connected model of 50 nodes, which is connected to H by only one edge. For comparison, define another network, N_0, composing of H only, without the small part S. Then, add some long-distance edges into H with probability p, so as to shorten the average network distance. Under this framework, the synchronizability of the networks N_0 and N_1 is analyzed numerically, with results as shown in Fig. 4.1a.

From Fig. 4.1a, one can observe the following: (1) Without the small part S, if p is increased, then λ_2 and λ_2/λ_N both rise up, implying that increasing p yields a better synchronizability of the network. (2) With the small part S, when p is large enough, λ_2 first increases and then saturates, while the largest eigenvalue λ_N continues to increase. Therefore, the ratio λ_2/λ_N eventually decays, thereby reducing the synchronizability. In other words, the network does not become more synchronizable, even though the probability p with long-distance connections increases, that is, the average network distance becomes smaller. This means that one cannot use the statistical properties to measure the synchronizability of networks in general, which is consistent with the observations reported in [15]. (3) It is easier for a network to synchronize in the case without the small community S than the case with S.

Furthermore, when there exists a small part S, as p is increased, the numerical result shows that the final value of the eigenvalue λ_2 remains to be about 0.021 (see Fig. 4.1a). In terms of (4.4), the theoretical value is $\lambda_2 \leq 2/50 = 0.04$, which is not of significant difference from the numerical result. In addition, when there exist two edges between H and S, the final value of λ_2 remains to be about 0.042 (see Fig. 4.1b), implying that the value of λ_2 is positively proportional to the number of edges between the two parts, at least for the present simple cases with one or two connections. In fact, this conclusion may also be deduced from (4.4).

4.3 Spectral Properties of Several Typical Networks

The spectrum of a network is the set of eigenvalues of the network's Laplacian matrix. While there are strict mathematical formulas to describe the spectra of some very regular networks, much less is known about the spectra of many real-world networks for their complex and irregular topological structures. A critical limitation in addressing the spectra of these real-world networks is the lack of theoretical tools for analysis; therefore, numerical simulation becomes the only way for investigation today.

For all the numerical results reported below, each value is obtained through averaging 50 simulation runs.

4.3.1 Regular Networks

Some very regular cases are easy to analyze.
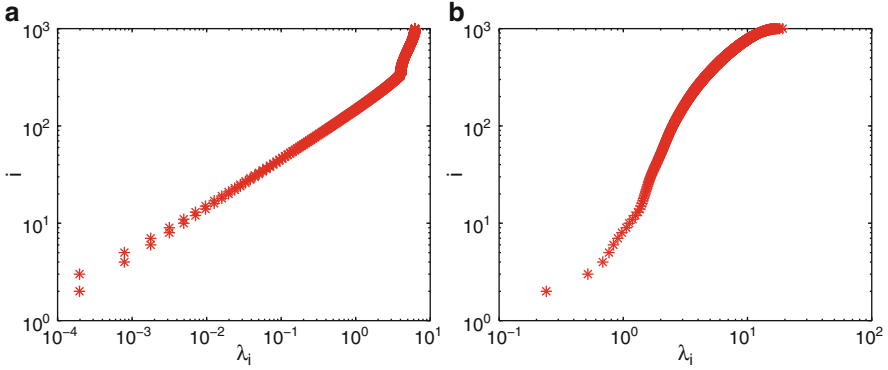
For a fully connected network, the Laplacian matrix is

$$L = \begin{pmatrix} N-1 & -1 & \cdots & -1 \\ -1 & N-1 & \cdots & -1 \\ \ddots & \ddots & \ddots & \ddots \\ -1 & -1 & \cdots & N-1 \end{pmatrix},$$

with eigenvalues

$$\lambda_1 = 0, \ \lambda_2 = \cdots = \lambda_N = N. \tag{4.5}$$

For a star-shaped network, the Laplacian matrix is

$$L = \begin{pmatrix} N-1 & -1 & -1 & \cdots & -1 \\ -1 & 1 & 0 & \cdots & 0 \\ \vdots & & & \ddots & \\ -1 & 0 & \cdots & 0 & 1 \end{pmatrix},$$

Fig. 4.2 Rank index i versus eigenvalues of the Laplacian matrices L: (**a**) $2K$-ring network with $N = 1000$ and $K = 2$; (**b**) random network with $N = 1000$ and $p = 0.007$

with eigenvalues

$$\lambda_1 = 0, \ \lambda_2 = \cdots = \lambda_{N-1} = 1, \ \lambda_N = N. \tag{4.6}$$

In a $2K$-ring network with degree sequence $\{2K, 2K, \ldots, 2K\}$, each node is connected to its $2K$ nearest neighbors, thereby forming a ring-shape of graph. Its Laplacian matrix is a circulant matrix:

$$L = \begin{pmatrix} 2K & -1 & \cdots & -1 & 0 & \cdots & 0 & -1 & \cdots & -1 \\ -1 & 2K & -1 & \cdots & -1 & & & & & \\ \ddots & \ddots & \ddots & \ddots & & & & & & \\ -1 & \cdots & -1 & 0 & \cdots & 0 & -1 & \cdots & -1 & 2K \end{pmatrix},$$

with eigenvalues 0 and $2K - 2\sum_{l=1}^{K} \cos \frac{2\pi i l}{N} = 4\sum_{l=1}^{K} \sin^2 \frac{\pi i l}{N}$, $i = 1, 2, \ldots, N - 1$.

To show some spectral properties of the $2K$-ring networks, consider the simple case of $K = 2$ as an example, and compute the eigenvalues of its Laplacian matrix for size $N = 1,000$. It can be seen from Fig. 4.2a that the nonzero eigenvalues come out equally in pairs, except the eigenvalue 4. Moreover, the smallest nonzero eigenvalue is $\lambda_2 = 0.00019739$ and the largest one is $\lambda_N = 6.25$. The eigenvalue ratio λ_2/λ_N is so small, implying that this network is very difficult to synchronize.

4.3.2 Random Networks

In contrary to the completely regular networks, a completely random network can be described by a random graph. One classical model of random graphs was first defined and then studied extensively by Erdös and Rényi [45]. An ER random
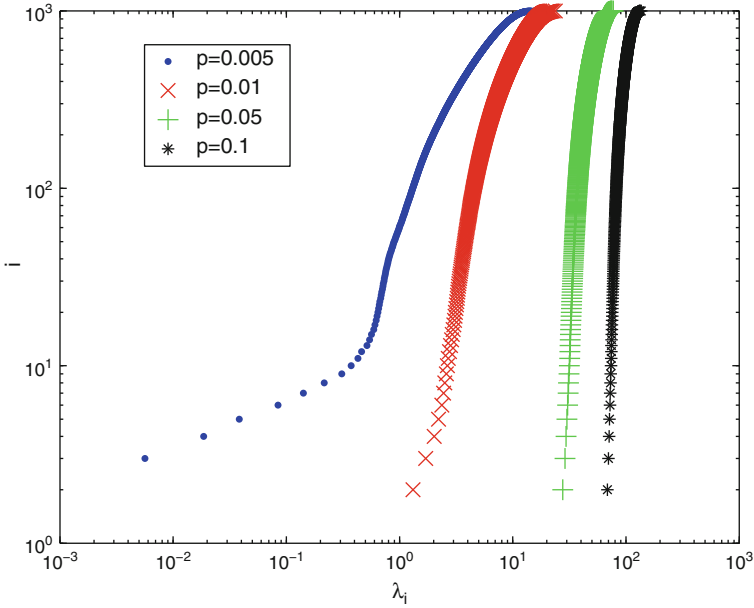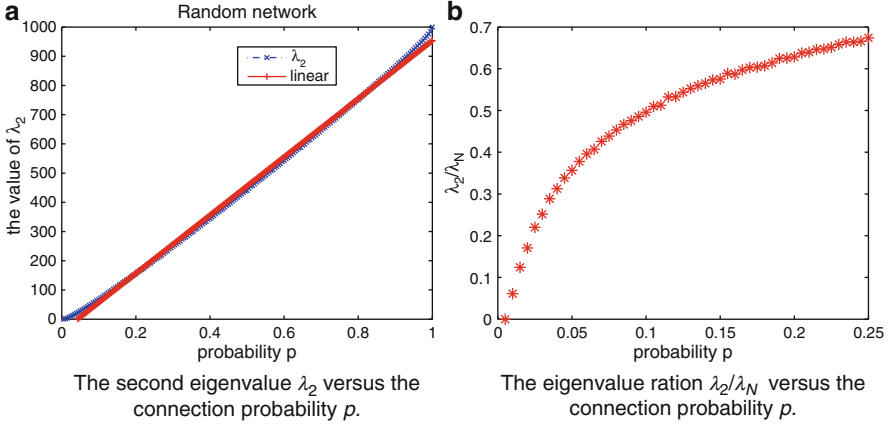
Fig. 4.3 Rank index i versus eigenvalues of the Laplacian matrices L, for random networks of size $N = 1,000$ with different connection probabilities

network has all edges established at random, with probability p, between each possible pair of nodes in the network. Thus, a random graph of N nodes with probability p will have $pN(N-1)/2$ edges statistically.

For example, consider such a network with $N = 1,000$ nodes. When $p = 0.007 > p_c$, where $p_c = (1+\varepsilon)\ln N/N \approx 0.0069$, the random network will almost surely be connected. The eigenvalues are uniformly distributed in the interval $[0, 20)$, as can be seen from Fig. 4.2b. The spectrum has a short span and is quite homogeneous. It is found that the smallest nonzero eigenvalue $\lambda_2 = 0.3712$ and the largest one is $\lambda_N = 19.0554$, giving the ratio $\lambda_2/\lambda_N = 0.0195$.

Figure 4.3 displays the spectra of random networks, which are changing with the connection probability p. One can observe that as p increases, the spectral width decreases quickly, meanwhile the smallest nonzero eigenvalue λ_2 and the largest one λ_N both increase. The main reason is that the increased p not only reduces the total number of isolated subgraphs, leading to increase of λ_2, but also raises the largest degree $d_{\max}$, indicating the increase of λ_N according to (4.1).

In the case of $p = 0.005$, the network has very sparse edges, and there exist some disconnected subgraphs, since $p < p_c$. Hence, $\lambda_2 = 0$, consistent with the numerical result. As a result, such random networks generated with $p = 0.005$ are impossible to synchronize in general. When $p = 0.01$, the smallest nonzero eigenvalue and the eigenvalue ratio are changed to $\lambda_2 = 1.4512$ and $\lambda_2/\lambda_N = 0.0610$, respectively. As the probability is further increased to $p = 0.1$, one has $\lambda_2 = 68.0447$ and the ratio

The second eigenvalue λ_2 versus the connection probability p.

The eigenvalue ration λ_2/λ_N versus the connection probability p.

Fig. 4.4 λ_2 and λ_2/λ_N of random networks of size $N = 1,000$ for different probabilities

becomes $\lambda_2/\lambda_N = 0.4979$. When the probability p is very close to 1, the model becomes very much like a fully connected network, and so the eigenvalue ratio λ_2/λ_N tends to 1. Therefore, from a statistical point of view, the synchronizability is enhanced gradually as the connection probability p is increased, as can be clearly seen from Fig. 4.4.

Interestingly, for random networks, a prominent approximately linear dependence between λ_2 and the connection probability p can be observed from Fig. 4.4a. Thus, $\lambda_2(p)$ is used to denote the dependence of λ_2 on the probability p. For a fixed size N, if $\lambda_2(p_1)$ and $\lambda_2(p_2)$ are computed from two suitable numbers of p_1 and p_2 ($p_1 \neq p_2$), then one can estimate the smallest nonzero eigenvalue $\lambda_2^*(p)$ for any p by using the following formula:

$$\lambda_2^*(p) \approx \frac{\lambda_2(p_1) - \lambda_2(p_2)}{p_1 - p_2}(p - p_1) + \lambda_2(p_1).$$

Since $p > p_c$, these random networks will almost surely be connected; therefore, it is reasonable to choose both $p_1, p_2 > p_c$. Here, take $p_1 = 0.1$ and $p_2 = 0.25$ to compute the corresponding λ_2^* of other probabilities p, resulting the plots shown in Fig. 4.5. It can be observed that the relative error $|\lambda_2 - \lambda_2^*|/\lambda_2$ is quite big when $p < 0.05$, while it is small when $p > 0.1$, and these estimations are almost exact.

4.3.3 Small-World Networks

Small-world networks are neither completely regular nor completely random; one representative model is the NW small-world network, proposed by Newman and Watts [46]. In this model, some edges are added to an initial $2K$-ring at random, with a probability $p \in [0, 1]$.
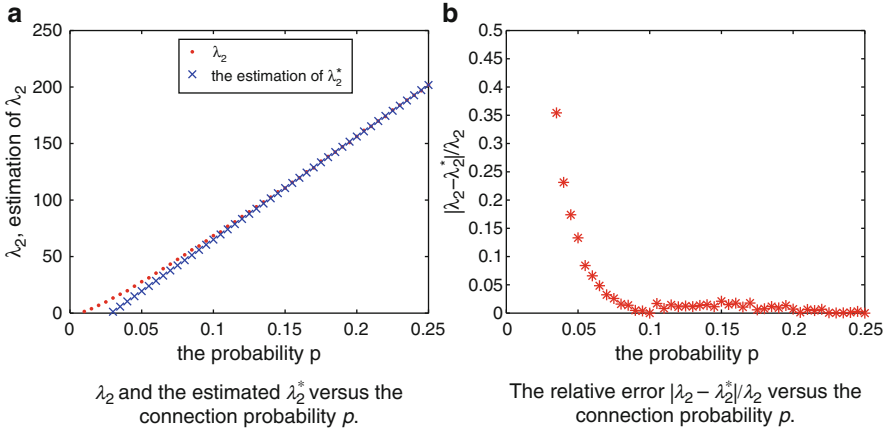
Fig. 4.5 The estimated λ_2^* and the relative error $|\lambda_2 - \lambda_2^*|/\lambda_2$ in random networks of size $N = 1,000$ for different connection probabilities
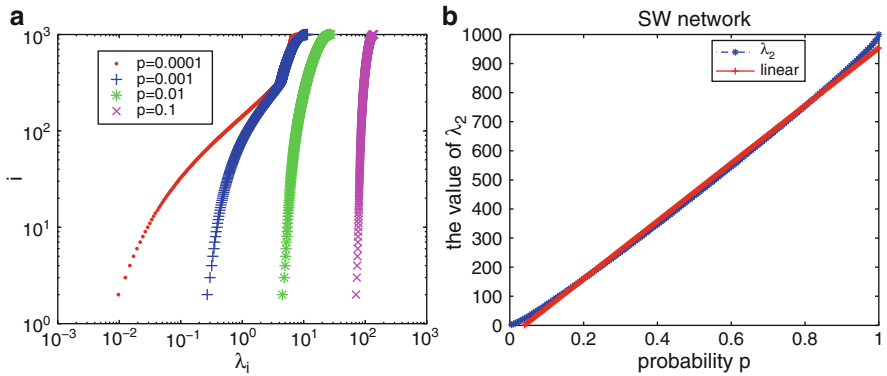
Fig. 4.6 Small-world networks of size $N = 1,000$: (**a**) Rank index i versus eigenvalues of Laplacian matrices L; (**b**) the smallest nonzero eigenvalue λ_2 versus the connection probability p

With $p = 0$, the network is the initial $2K$-ring network. As p is increased, the smallest nonzero eigenvalue λ_2 and the largest one λ_N both will increase (see Fig. 4.6a). However, λ_2 grows much faster than λ_N, resulting in an increased eigenvalue ratio λ_2/λ_N. It implies that the synchronizability of the small-world network is improved as the connection probability is increased.

For $0 < p < 1$, it can be seen from Figs. 4.3 and 4.6a that, similarly to random networks, the spectral range of a small-world network becomes narrower when the connection probability p is increased.

With $p = 1$, the small-world model becomes a fully connected graph, so the spectrum of this case is similar to the fully connected network discussed before.

Thus, it can be concluded that the spectrum of an NW small-world network, which is quite homogeneous, transits from the spectrum of a $2K$-ring network to that of a fully connected network, as the connection probability p is increased.

For the NW small-world network model, a similar phenomenon of a prominent approximately linear dependence of λ_2 on the connection probability p can be observed, as seen from Fig. 4.6b. By linear fitting, the estimation of λ_2 for an NW small-world network of $N = 1,000$ can be obtained, as $\lambda_{2\mathrm{nw}}^*(p) = 992.48 * p - 38.831$. It should be noted that these values are related to several parameters such as the probability p, the ring constant K, and the size N of the network.
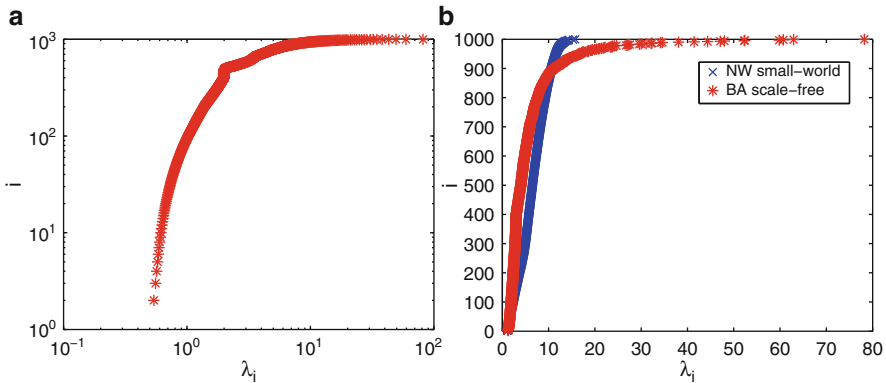
4.3.4 Scale-Free Networks

Scale-free networks are characterized by the power-law form of their degree distributions, which can be generated with the Barabási–Albert's preferential attachment algorithm [47]. Staring from an initial set of m_0 fully connected nodes, one node is added along with m new edges, at every time step. Nodes in the existing network with higher degrees have higher probabilities, proportional to their degrees, to be connected by the new node through a new edge, where multiple connections are prohibited. This algorithm yields a typical BA scale-free network, which is growing until the process stops.

Figure 4.7a shows some spectral properties of a scale-free network of size $N = 1,000$. It can be seen that the eigenvalues are distributed in a very heterogeneous way. Part of the eigenvalues are located in the interval $[0, 20]$, while some larger ones are located far away from this interval. The smallest nonzero eigenvalue is $\lambda_2 = 0.5391$ and the largest one is $\lambda_N = 81.6367$, resulting in the ratio $\lambda_2/\lambda_N = 0.0066$. It can also be observed that a large difference exists between λ_2 and λ_N, implying that the spectral distribution range of the scale-free network is wide, distinctive from regular, random and small-world networks.

Figure 4.7b compares the spectra between NW small-world and BA scale-free networks. It can be seen that the span of the eigenvalues distribution in the small-world network is smaller than that of the scale-free network. For the latter, most of its eigenvalues are comparatively concentrated, and meantime there are some very large eigenvalues.

In summary, the spectral properties of different networks are clearly different. Thus, one can tell which category a network belongs to, by simply looking at its spectral properties. The spectra of regular, random, and small-world networks are homogeneous, whereas those of scale-free networks are heterogeneous. Furthermore, for random and small-world networks, the synchronizability is increased as the connection probability p is increased. In particular, the smallest nonzero eigenvalue is almost linearly dependent on the connected probability for both ER random and NW small-world networks.

Fig. 4.7 Rank index i versus Eigenvalues of the Laplacian matrices L: (**a**) scale-free networks with $N=1{,}000$, $m_0=5$ and $m=2$; (**b**) scale-free networks with $N=1{,}000$, $m_0=5$ and $m=3$, and small-world networks with $N=1{,}000$ and $p=0.0025$

4.3.5 Community Networks

Community structure means densely connected groups of nodes with sparse connections between them. This section discusses the spectra of networks with prominent community structures, called community networks.

First, consider the spectra of networks composing of two communities, each of which is (1) a fully connected graph (Fig. 4.8a); (2) a random network (Fig. 4.8b); (3) a small-world network (Fig. 4.8c); and (4) a scale-free network (Fig. 4.8d). There are some random edges between two communities. It can be seen from Fig. 4.8 that there is a big gap between λ_2 and λ_3. Moreover, as the number of edges between two communities is increased, λ_2 is increased and the gap between λ_2 and λ_3 decreases, indicating that the community structure becomes blurred. It can also be seen that the other eigenvalues basically remain unchanged, reflecting the robustness of the spectral properties of the corresponding subgraphs.

Next, consider some networks composing of three communities: (1) each community is a small-world network (Fig. 4.9a); (2) each community is a scale-free network (Fig. 4.9b). There exist several random edges between every two communities. It can be seen that there is a big gap between λ_3 and λ_4, and the increased number of random edges among the three communities led to the increased values of λ_2 and λ_3. Furthermore, λ_2 and λ_3 are increased much faster than the other eigenvalues; therefore, the difference between λ_3 and λ_4 is reduced, and the community structure becomes blurred.

Remark 4.1. From Figs. 4.8c (4.9a), namely, and 4.8d (4.9b), one can find that the distributions of the eigenvalues in Figs. 4.8c and 4.9a are more homogeneous than those shown in Figs. 4.8d and 4.9b. This is probably due to the heterogeneity of the BA scale-free subnetworks and the homogeneity of the NW small-world
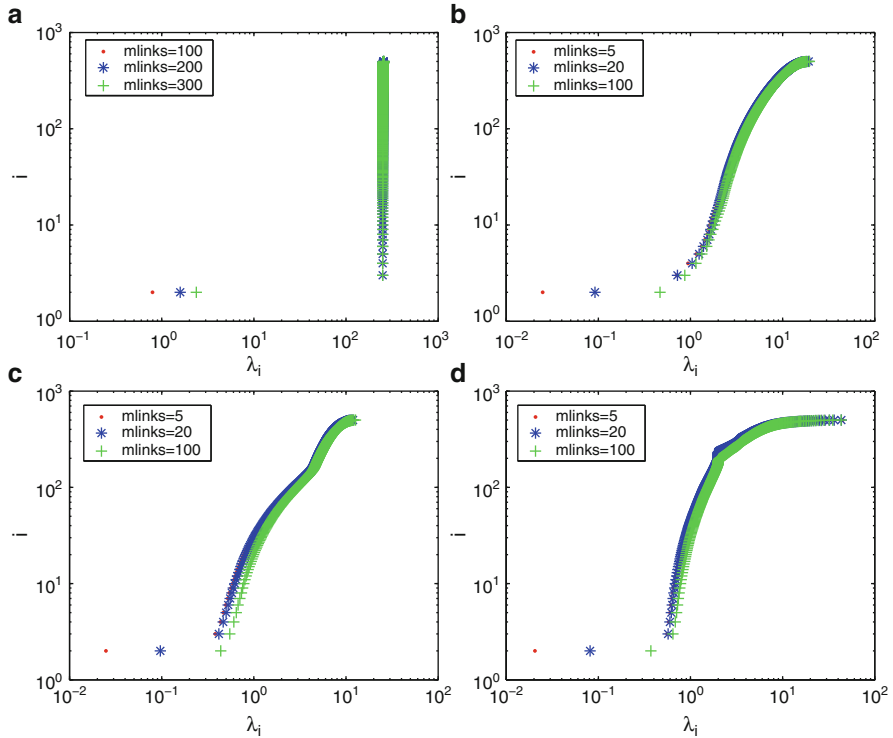
Fig. 4.8 Rank index i versus eigenvalues of the Laplacian matrix L: (**a**) a network composing of two fully connected subgraphs of size $N = 250$, with random edges 100, 200 and 300 between two communities, respectively; (**b**) a network composing of two random subgraphs of size $N = 250$, with $p = 0.03$, having 5, 20 and 100 random edges between two communities, respectively; (**c**) a network composing of two small-world subgraphs of size $N = 250$, with $p = 0.005$, having 5, 20 and 100 random edges between two communities, respectively; (**d**) a network composing of two scale-free subgraphs of size $N = 250$, with $m_0 = 5$ and $m = 2$, having 5, 20 and 100 random edges between two communities, respectively

subnetworks, since there exists a positive correlation between the spectrum and the degree sequence, as will be further discussed later in Sect. 4.4. Thus, the more diverse the degree distribution, the more heterogeneous the eigenvalues of the BA scale-free subnetworks.

In summary, the spectra of community networks bring to light many aspects of the network topologies: (1) the number of zero eigenvalues equals the number of isolated communities; (2) a gap between eigenvalues indicates the existence of a community structure; (3) for a network with k prominent communities, there are $k - 1$ eigenvalues near zero, the gap between λ_k and λ_{k+1} is larger than the difference between any other consecutive eigenvalues, and larger eigenvalues in the last part of the sequence reflect some major properties of communities; and (4) the increase of the number of edges between communities can result in the increase of the value of λ_2, which also means a better synchronizability.
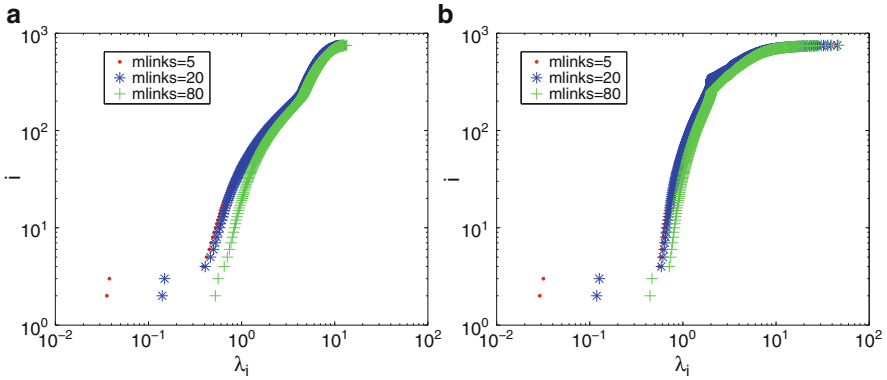
Fig. 4.9 Rank index i versus eigenvalues of the Laplacian matrix L: (**a**) a network composing of three small-world subgraphs of size $N = 250$, with $p = 0.005$, 5, 20, and 80, respectively, having random edges between two communities; (**b**) a network composing of three scale-free subgraphs of size $N = 250$, with $m_0 = 5$ and $m = 2$, 5, 20, and 80, respectively, having random edges between two communities

4.4 Relation Between the Spectrum and the Degree Sequence

Real-world networks are usually very large in size; thus, it is generally difficult and time-consuming to compute their spectra. However, the degree sequence is easy to obtain. So, if one can find the relation between a spectrum and a degree sequence, it will be reasonable to make use of the degree sequence for estimating the spectrum of a real network. The question is, then, whether or not they have any easily described and computable relations?

4.4.1 Theoretical Analysis

In order to identify some intrinsic relations between the Laplacian eigenvalues and the degree sequence of a network, the following lemma is needed.

Lemma 4.1 (Wielanelt-Hoffman Theorem [48]). *Suppose $C = A + B$, where $A, B, C \in R^{N \times N}$ are symmetric matrices, and let the eigenvalue sets $\lambda(B)$ and $\lambda(C)$ be arranged in the non-decreasing order. Then,*

$$\sum_{i=1}^{N} |\lambda_i(C) - \lambda_i(B)|^2 \leq ||A||_F^2,$$

where $||A||_F = \left(\sum_{ij} |a_{ij}|^2 \right)^{1/2}$ denotes the Frobenius norm of matrix A.

Theorem 4.1 ([49]). *Let G be a graph of N nodes with Laplacian matrix L, and arrange the node-degree set and the eigenvalue set in the vector form, as $d = (d_1, d_2, \ldots, d_N)^{\mathrm{T}}$ and $\lambda(L) = (\lambda_1, \lambda_2, \ldots, \lambda_N)^{\mathrm{T}}$, respectively, both in the non-decreasing order. Then,*

$$\delta = \frac{||\lambda(L) - d||_2}{||d||_2} \leq \frac{\sqrt{||d||_1}}{||d||_2} \leq \sqrt{\frac{N}{||d||_1}}.$$

Remark 4.2. Theorem 4.1 shows that for the Laplacian matrix L, the difference between Laplacian eigenvalues $\lambda(L)$ and node-degrees d is bounded by $||d||_1/||d||_2^2$. Thus, for a large-scale complex network with a huge number of edges, $||d||_1/||d||_2^2$ typically have a small value, implying that the distribution of the Laplacian eigenvalues is indeed similar to the distribution of the node degrees. On the other hand, however, for a large-scale network with sparse connections, the value of $N/\left(\sum_{i=1}^{N} d_i\right)$ is usually small, implying that the inequality is quite conservative.

Remark 4.3. It is reported in [49] that the differences between Laplacian eigenvalues $\lambda(L)$ and node-degrees d are very small for random, small-world and scale-free networks, according to extensive numerical simulations. In the next subsection, it will be shown that the eigenvalues distributions are very closely related to the node-degree sequences, which is consistent with the results of [49].

Theorem 4.2 ([49]). *Let λ_j be the eigenvalues of the Laplacian matrix L of a graph with N nodes, and d_i be the degree of node i, $i = 1, 2, \cdots, N$. Then, in every interval $[d_i - \sqrt{d_i}, d_i + \sqrt{d_i}]$, there is at least one eigenvalue $\lambda^* \in \{\lambda_j | j = 1, 2, \ldots, N\}$ of L, that is,*

$$(d_i - \sqrt{d_i}) \leq \lambda^* \leq (d_i + \sqrt{d_i}), \quad i = 1, 2, \cdots, N.$$

Remark 4.4. In Theorem 4.2, some intervals $[d_i - \sqrt{d_i}, d_i + \sqrt{d_i}]$ may overlap, and some eigenvalues of L may not fall into any of such intervals at all.
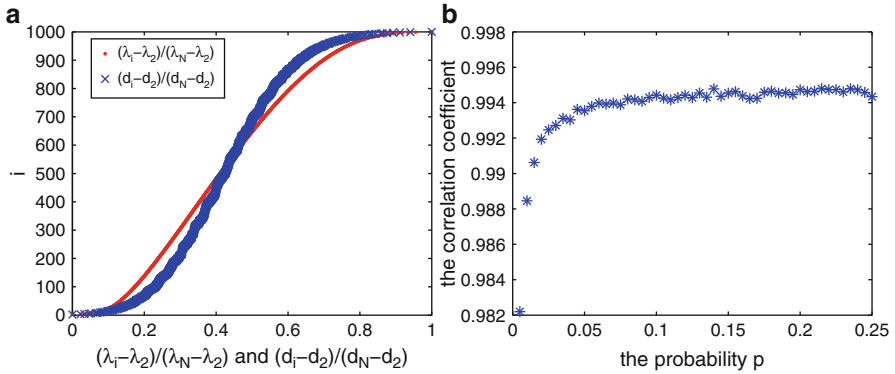
Remark 4.5. By the Gerschgorin Theorem, the eigenvalues of L satisfy that

$$|\lambda - l_{ii}| \leq \sum_{j=1, j \neq i}^{N} |l_{ij}|.$$

Since $l_{ii} = d_i$, and L has zero row-sum, one has $|\lambda - d_i| \leq d_i$, namely,

$$0 \leq \lambda \leq 2d_i, \quad i = 1, 2, \ldots, N.$$

Thus, one can see that the result given by Theorem 4.2 is less conservative than this estimation given by the Gerschgorin Theorem.

Fig. 4.10 ER random networks of size $N = 1,000$: (**a**) rank index i versus the relative spectrum and relative degree sequence, when $p = 0.0258$; (**b**) correlation coefficient between the spectrum and degree sequence versus the probability p

4.4.2 Numerical Results

To visualize the relation between the eigenvalues distribution and the degree sequence, extensive numerical simulations were performed and analyzed.

For convenience of analysis, define the relative spectrum

$$R_e(i) := (\lambda_i - \lambda_2)/(\lambda_N - \lambda_2), \ i = 2, 3, \ldots, N,$$

and the relative degree sequence

$$R_d(i) := (d_i - d_2)/(d_N - d_2), \ i = 1, 2, \ldots, N.$$

Numerical results illustrated in Figs. 4.10a, 4.11a and 4.12a show the relations between the relative spectrum R_e and the relative degree sequence R_d. The total numbers of edges, in the random networks with $p = 0.0258$, the small-world networks with $p = 0.0218$, and the scale-free networks with $m_0 = m = 13$, are all equal to 12909 ± 10.

It can be easily seen from Fig. 4.10a that the spectrum and the degree sequence of a random network seems to be correlated, but how much the two are correlated is unclear, so the correlation coefficient between the spectrum and the degree sequence is calculated. When the connection probability $p = 0.0258$, from Fig. 4.10b, one can see that the correlation coefficient is 0.9925. That is, the spectrum and degree sequence are quite correlated. And, the correlation coefficient is increased, though slowly, as p is increased.

Figure 4.11a shows the correlation between the spectrum and degree sequence of a small-world network of 1,000 node with the connection probability $p = 0.0218$. Calculation yields the correlation coefficient 0.9921 in this case, implying that the spectrum and degree sequence are comparatively correlated. Fig. 4.11b shows that
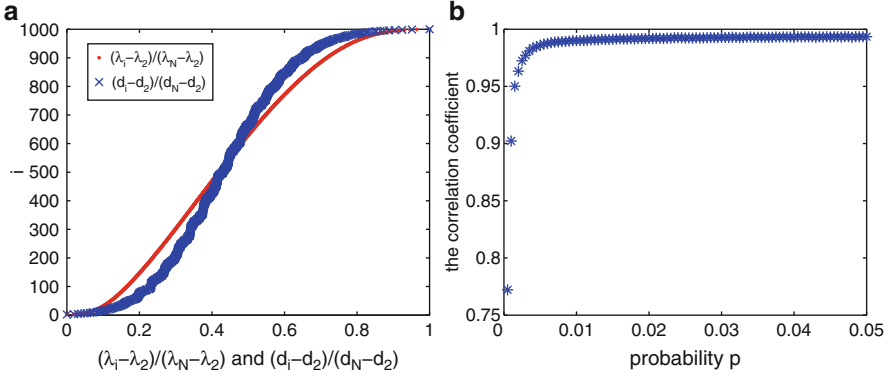
Fig. 4.11 NW small-world networks of size $N = 1,000$: (**a**) rank index i versus the relative spectrum and relative degree sequence, when $p = 0.0218$; (**b**) correlation coefficient between the spectrum and degree sequence versus the probability p
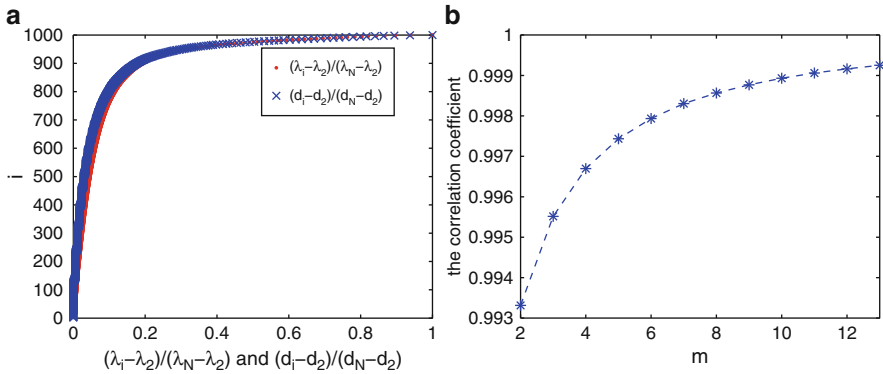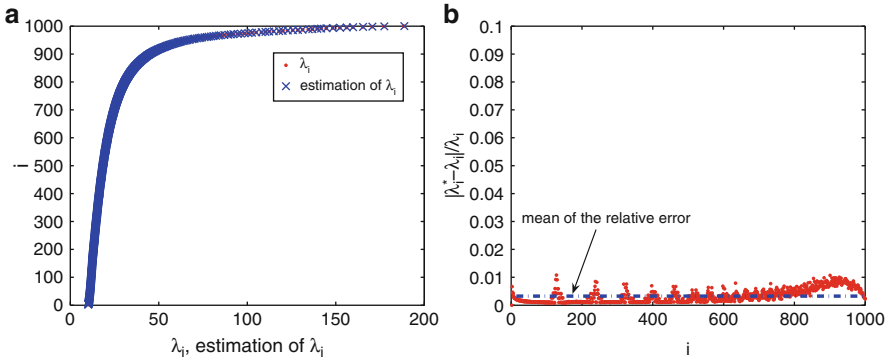

Fig. 4.12 BA scale-free networks of size $N = 1,000$: (**a**) rank index i versus the relative spectrum and relative degree sequence of scale-free networks of size $N = 1,000$, when $m_0 = m = 13$; (**b**) correlation coefficient between the spectrum and degree sequence versus m

the correlation coefficient ascends to a certain degree, and then converges to a constant value of 0.9935 as the probability p is increased further.

From Fig. 4.12, one can see that the spectrum and degree sequence of a BA scale-free network are closely correlated. Indeed, when $m_0 = m = 13$, the correlation coefficient equals 0.9992. Figure 4.12b shows the increasing correlation coefficient with the increasing m.

Moreover, it can also be observed that the correlation between the spectrum and degree sequence of a scale-free network is the highest, followed by random networks and then by small-world networks. Therefore, in the following, a scale-free network with $m_0 = m = 13$ is used as an example to estimate all the eigenvalues in terms of λ_2, λ_N, and the degree sequence.

Fig. 4.13 Scale-free networks of size $N = 1,000$: (**a**) λ_i and the estimation λ_i^* versus the rank index i; (**b**) λ_i and the estimation λ_i^* versus the rank index i

It is known that if the correlation coefficient between two random variables X, Y is close to 1, then it means that the probability of the linear relation $Y = aX + b$ is close to 1. But the parameters a and b are usually unknown, so it is difficult to compute the whole spectrum of eigenvalues (the so-called global method) from the degree sequence, λ_2 and λ_N. The following is an efficient local algorithm for computing approximations of λ_{i+1} from λ_i, $i = 1, 2, ..., N$.

- Initial conditions: $\bar{\lambda}_1 = \lambda_1^* = 0$.
- Step 1 (Prediction). Compute $\bar{\lambda}_i$ in terms of the degree sequence, λ_2, and λ_N, as follows:

$$\bar{\lambda}_i = \frac{d_i - d_2}{d_N - d_2}(\lambda_N - \lambda_2) + \lambda_2.$$

- Step 2 (Correction). Compute the approximation λ_{i+1}^* from λ_i, iteratively, by

$$\lambda_{i+1}^* = \lambda_i + (\bar{\lambda}_{i+1} - \bar{\lambda}_i), \; i = 1, 2, \ldots, N - 1.$$

Figure 4.13a shows a comparison between the approximated λ_i^* and the exact λ_i, $i = 2, 3, \ldots, N$. It is clear that the estimations are very accurate. From Fig. 4.13b, one can see that the relative error $(\lambda_i - \lambda_i^*)/\lambda_i$ is very small, with an average of 0.3263%, demonstrating that the local algorithm for estimating λ_{i+1} from λ_i is indeed highly effective.

4.5 Synchronization Processes on Complex Networks

Complex networks in various physical systems can be described at different scales. This section discusses networks at the "mesoscale," as defined in [25], addressing subgraphs rather than at the "microscale" which addresses individual nodes or at

the "macroscale" which addresses the network as a whole. The mesoscale is an intermediate scale examining substructures such as motifs, cliques, cores, loops, and communities. In particular, the community detection problem concerning the determination of mesoscopic structures that have functional, relational or even social dynamics and impacts is an important and yet also challenging subject for investigation in the field of complex networks.

This section focuses only on synchronization processes on complex networks at the mesoscale level of description. Synchronization is a generic feature of networked dynamical systems such as cells and oscillators. Previous studies have discussed the onset of synchronization and the impact of structural properties on network synchronizability. The interest here is the regions outside the onset of phase synchronization and the role of network topology in the synchronization processes.

4.5.1 Paths to Synchronization on Complex Networks

One of the most popular models for coupled oscillators is the Kuramoto model [50]:

$$\frac{\mathrm{d}\theta_i}{\mathrm{d}t} = \omega_i + \lambda \sum_{j=1}^{N} A_{ij} \sin(\theta_j - \theta_i), \; i = 1, 2, \ldots, N, \tag{4.7}$$

where ω_i represents the natural frequency of the ith oscillator and λ is the coupling constant.

This model can be studied in terms of an order parameter, r, that measures the extent of phase synchronization in the network, defined by

$$r\mathrm{e}^{\mathrm{i}\Psi} = \frac{1}{N} \sum_{j=1}^{N} \mathrm{e}^{\mathrm{i}\theta_j},$$

where Ψ represents the average phase of the network. The parameter $0 \leq r \leq 1$ displays a second-order phase transition in the coupling strength, with $r = 0$ being the value of the incoherent solution and $r = 1$ the value of the complete phase synchronization.

In [26], a new parameter, r_{edge}, is defined, as

$$r_{\mathrm{edge}} = \frac{1}{2N_l} \sum_{i} \sum_{j \in \Gamma_i} \left| \lim_{\Delta t \to \infty} \int_{t_{\mathrm{r}}}^{t_{\mathrm{r}} + \Delta t} \mathrm{e}^{\mathrm{i}[\theta_i(t) - \theta_j(t)]} \mathrm{d}t \right|,$$

where Γ_i is the set of neighbors of node i and N_l is the total number of edges. This parameter represents the fraction of edges with which the network achieves phase synchronization, averaging over a large enough time interval Δt after the network is relaxed at a large time instant t_{r}.

In [26], the dynamics of (4.7) for ER and scale-free (SF) networks were studied, with respect to both global and local synchronization. It shows that the evolution
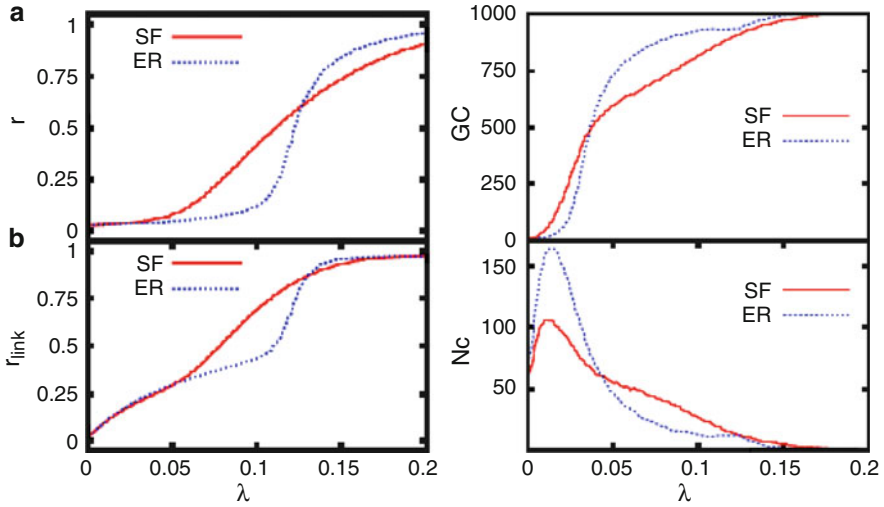
Fig. 4.14 *Left*: evolution of the order parameter r, and the fraction of synchronized edges $r_{link}(=r_{edge})$ as a function of λ; *Right*: size of the largest synchronized connected component (GC) and the number of synchronized connected components (N_C), as a function of λ, for the different topologies considered [26]

of the order parameter r, as λ increases, can capture the global coherence of synchronization in the network, and that r_{edge} can be used to measure the local formation of synchronization patterns thereby revealing how global synchronization is achieved.

Synchronization processes in ER and SF networks were studied numerically in [26]. It can be seen from Fig. 4.14 that the global coherence of the synchronized state, represented by r and implying the onset of synchronization, first occurs for the SF network. If λ is further increased, there is a value of r for the ER network curve to cross over the SF network curve. From this value up, in λ, the ER network remains slightly better in synchrony than the SF network. The behavior of r_{edge} provides some additional information about the processes between ER and SF networks. Interestingly, the nonzero values of r_{edge} for very small λ indicate that some local synchronization patterns has occurred even in the regime of global incoherence ($r \approx 0$). Right at the onset of synchronization for the SF network, its r_{edge} value grows faster than the ER network. This implies that for the SF network the locally synchronized structures rise at a faster rate than the ER network. Finally, when λ is further increased, for the ER network, the growth in its synchronization patterns increases drastically up to those obtained from the SF network, and even higher.

From the evolution of the number of synchronized clusters and the size of the largest generated clusters (GC) shown in Fig. 4.14, the emergence of clusters of synchronized pairs of oscillators (edges) in the networks shows that for small λ values, still in the incoherent range with $r \approx 0$, both ER and SF networks have developed a largest cluster of synchronized pairs of oscillators involving about 50%

Fig. 4.15 Correlation between the likelihood that a node belongs to the GC of pairs of synchronized oscillators and its degree k as a function of the coupling strength λ in the SF network [26]
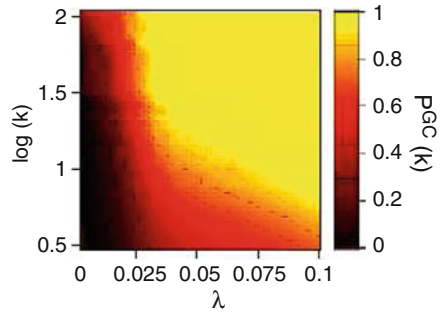
of the network nodes, with an equal number of smaller synchronization clusters. From this point of view, in the SF network the GC grows up but the number of smaller clusters goes down, whereas for the ER network the growth exploits. These results indicate that although SF networks present more coherence in terms of both r and r_{edge}, the mesoscopic evolution of the synchronization patterns is slower than the ER networks, which are far more locally synchronizable than heterogeneous networks in general (see [26]).

In [26], it argued that the above observed differences in the local behavior are resulted from the growth of the GC. It is shown in [26] that for ER networks pairs of oscillators synchronize to merge and form many different clusters and then form a GC when the coupling strength is increased. Many small clusters join together to produce a giant component consisting of synchronized pairs, the size of which is almost the same as the whole network, as soon as the global coherent state is achieved. However, this is far from the case for SF networks, where the GC is formed from a core consisting of about a half of the nodes in the network, and then new pairs of oscillators are incorporated into the GC one by one, as the coupling strength is increased.

In Fig. 4.15, it can be seen that for the SF network, the probability that a node of degree k belongs to the GC is an increasing function of k for every fixed λ, hence the more connected a node is, the more likely it takes part in the cluster of synchronized entries, as reported in [26]. Therefore, one can conclude that synchronization starts from the node with the largest degree and then spreads to the rest nodes in the network in this scenario.

Remark 4.6. The observed phenomena may be understood from the master-stability-function point of view. In this setting, the dynamics of a network of N coupled oscillators is described by

$$\dot{x}_i(t) = f(x_i(t)) - \varepsilon \sum_{j=1}^{N} L_{ij}\Gamma x_j, \ i = 1, 2, \ldots, N, \tag{4.8}$$

where x_i is the state of oscillator i and $f(x_i(t))$ governs its dynamics, Γ is the inner coupling matrix, and $L = (L_{ij})$ is the Laplacian matrix of the network. Denote the

completely synchronizing state of (4.8) as $\{x_j(t) = s(t),\ \forall j\,|\,\dot{s}(t) = f(s(t))\}$. A small perturbation on $s(t)$ yields the following linear variational equations:

$$\dot{\delta}x_i(t) = Df(s(t))\delta x_i - \varepsilon \sum_{j=1}^{N} L_{ij}\Gamma(\delta x_j),\ i = 1,2,\ldots,N. \tag{4.9}$$

Further, (4.9) can be diagonalized into N decoupled blocks of the form

$$\dot{\eta}_i = [Df(s(t)) - \varepsilon\lambda_i\Gamma]\eta_i,\ i = 1,2,\ldots,N. \tag{4.10}$$

From (4.10), the speed of node i converging to the synchronization manifold is mainly determined by λ_i, with $f(\cdot)$ given. It has been shown in the above that the distribution of the Laplacian eigenvalues of a network is strongly related to the node-degree distribution; therefore, one can conclude that synchronization typically starts from the node with the largest degree.

4.5.2 Paths to Generalized Synchronization on Complex Networks

In [32], the processes of generalized synchronization (GS) of complex networks was studied, mainly on NW small-world networks and BA scale-free networks, using the adaptive coupling strategy in the following form:

$$\dot{x}_i = f_i(x_i(t)) - c_i(t) \sum_{j=1}^{N} a_{ij}\Gamma(x_i(t) - x_j(t)), \qquad i = 1,2,\ldots,N, \tag{4.11}$$

where x_i is the state of node i, $f_i(\cdot)$ is a continuous vector function, $c_i(t) > 0$ is a time-varying coupling strength to be designed using only the neighborhood information of node i, Γ is the inner coupling matrix, and $A = (a_{ij})$ is the adjacency matrix of the network.
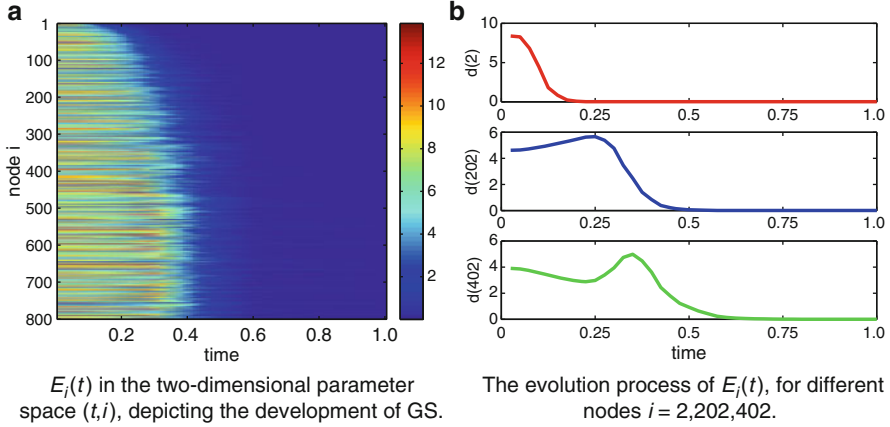
Construct an auxiliary network of the form

$$\dot{x}'_i = f_i(x'_i) - c_i(t) \sum_{j=1}^{N} a_{ij}\Gamma(x'_i - x_j), \qquad i = 1,2,\ldots,N, \tag{4.12}$$

denote $e_i = x'_i - x_i$, and apply the adaptive controller

$$\dot{c}_i(t) = \gamma_i \sum_{j=1}^{N} a_{ij}e_i^T\Gamma e_i, \qquad i = 1,2,\ldots,N, \tag{4.13}$$

where γ_i are positive constants.

a

$E_i(t)$ in the two-dimensional parameter space (t,i), depicting the development of GS.

b

The evolution process of $E_i(t)$, for different nodes $i = 2, 202, 402$.

Fig. 4.16 Visualization of the evolutionary process to reach global GS via adaptive coupling strength regulation on a BA network. Total number of nodes $N = 800$ and total number of edges is 2388 ± 2 [32]

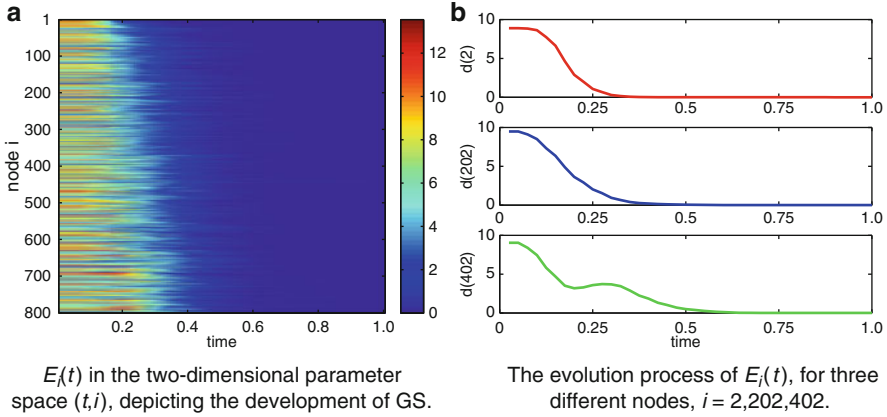To describe the process of GS on network (4.11), define the following error signals at each time step:

$$E_i(t) = ||x_i'(t) - x_i(t)||_2, \qquad i = 1, 2, \ldots, N, \qquad (4.14)$$

and label the nodes according to their decreasing degree ordering $d(1) \geq d(2) \geq \cdots \geq d(N)$. Thus, $i = 1$ denotes the node with the largest degree, $i = 2$ the node with the second largest degree, and so on.

Numerical results illustrated by Figs. 4.16 and 4.17 show the processes towards global GS. Figure 4.16a shows the synchronization process of a BA network with $m = 3$; Fig. 4.16b displays the evolution process of $E_i(t)$, with $i = 2, 202$ and 402, respectively, for $t \in [0, 1.0]$. Figure 4.17a shows the synchronous process of a NW network, with connection probability $p = 0.0025$; Fig. 4.17b displays the evolution process of $E_i(t)$, with $i = 2, 202$, and 402, respectively, for $t \in [0, 1.0]$. The total numbers of edges in the BA network and the NW network are both equal to 2388 ± 2.

Clearly, not all nodes can achieve a common GS state simultaneously. Also obviously, there is a transition process from non-GS to global GS. It can be seen from Fig. 4.16a that, as time evolves, GS starts from the nodes with the largest degree and then spreads to the rest of the network. This can also be verified by (4.11)–(4.12), from which linearization results in

$$\dot{e}_i = \left[Df_i(x_i) - c_i(t) \sum_{j=1}^{N} a_{ij} \Gamma \right] e_i, \qquad (4.15)$$

a

$E_i(t)$ in the two-dimensional parameter
space (t,i), depicting the development of GS.

b

The evolution process of $E_i(t)$, for three
different nodes, $i = 2, 202, 402$.

Fig. 4.17 Visualization of the process to global GS via adaptive coupling strength regulation of a NW network. The total number of nodes $N = 800$ and the total number of edges is 2388 ± 2 [32]

a

b
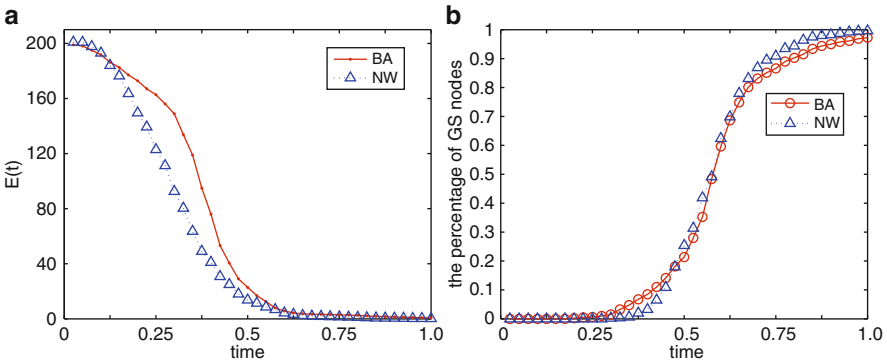
Fig. 4.18 A comparition of BA network and NW network. (**a**) shows the evolution of the total errors $E(t)$; (**b**) shows the percentage of nodes which have achieved GS in the adaptive evolution process [32]

where $Df_i(x_i)$ denotes the Jacobian matrix of $f_i(x)$ at x_i. In (4.15), $\sum_{j=1}^{N} a_{ij}$ is the degree of node i; hence, the larger a node's degree is, the faster its synchronization error converges, as can be seen in Figs. 4.16b and 4.17b.

Next, define $E(t) = \sum_{i=1}^{N} E_i(t)$.

Figure 4.18a shows the evolution of $E(t)$ for a BA scale-free network and a NW small-world network, while Fig. 4.18b shows the percentage of synchronized nodes in the GS process.

From Fig. 4.18, one can see that the BA network is easier to reach GS in the early stage, but harder in the later stage, in the process. This can be explained by the fact that the NW network has a comparative homogeneous node-degree distribution while the BA network has some hubs with extremely large degrees. In fact, in the

beginning of the process, the existence of these hubs accelerates the GS speed on the BA network. But, at the later stage, the speed to achieve GS is dominated by the large number of nodes with smaller degrees. Thus, for the BA network, although the hubs achieve GS rather quickly, the distant nodes are much more difficult to achieve GS. So, as a result on the whole large network, it is easier for the NW network to achieve global GS than the BA network with the same numbers of nodes and edges.

4.5.3 Paths to Synchronization on Community Networks

In this subsection, synchronization processes on community networks are investigated.

Again, consider the network of N coupled identical oscillators, described by (4.7) with $\omega_i = \omega$, $\forall i$. The objective is to achieve $\theta_i \to \theta$, $\forall i$ as $t \to \infty$. This problem was studied in [24, 25], where the following concepts were defined to characterize the dynamic time scales:

- The average of the correlations between pairs of oscillators

$$\rho_{ij}(t) = \langle \cos(\theta_i(t) - \theta_j(t)) \rangle, \tag{4.16}$$

 where the brackets stand for the average over initial random phases;
- A connectively matrix with a given threshold T based on the above average correlations between pairs of oscillators

$$\mathscr{D}_T(t)_{ij} = \begin{cases} 1 & \text{if } \rho_{ij}(t) > T, \\ 0 & \text{if } \rho_{ij}(t) < T. \end{cases} \tag{4.17}$$

  For large enough T, the evolution of this matrix unravels the process of nodes merging into groups or communities.

In this part, a community network is composed of a huge part H and a small part S, where H is a NW small-world model of 500 nodes with connection probability $p = 0.01$, and S is a fully connected model of 50 nodes and is connected to H via only one edge. Through numerical simulations, some relation between the dynamic time scales and the Laplacian spectrum are obtained, as shown in Fig. 4.19.

In Fig. 4.19a, one can see the evolution of the oscillators, and find a path to the final global complete synchronization on a community network. When time $t < 0.02$, the whole network is in the state of "non-synchronization." As time goes on, the nodes in the small community S begin to synchronize, while those in the huge community H do not. This situation is referred to as "partial synchronization," which is determined by the community topological structure, where nodes inside the communities are first to synchronize. The small community S is fully connected, so is easier to synchronize than the huge one H. When $t > 0.5$, the nodes in

a

b

c

d
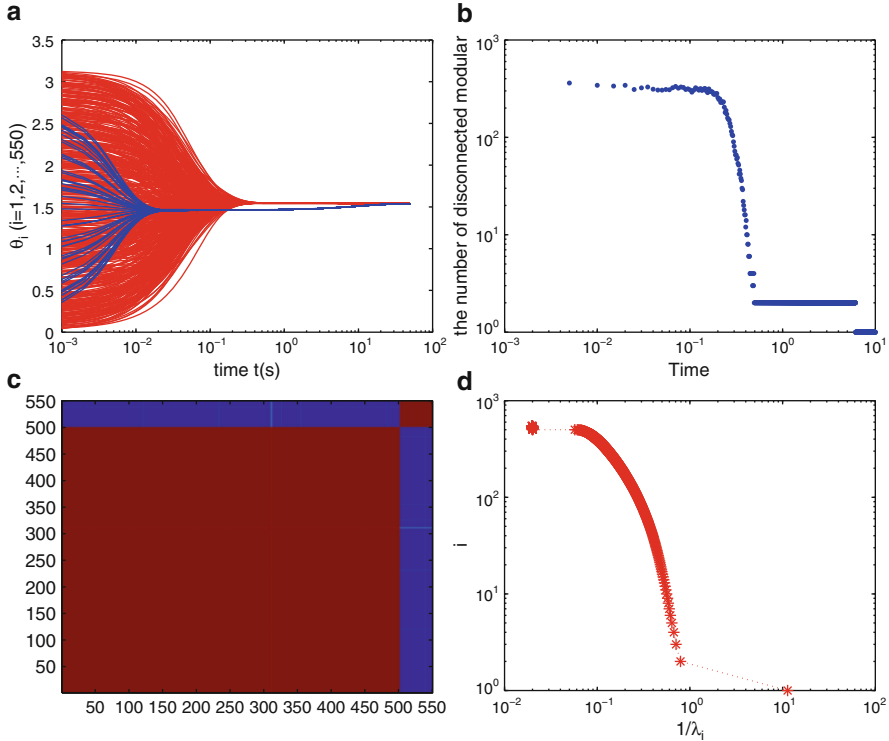
Fig. 4.19 Network with two communities: one is a huge part H of a small-world model of 500 nodes with $p = 0.01$; another is a small part S of a fully connected model of 50 nodes; with only one edge linking the two communities. (**a**) The time evolution of oscillators θ_i $(i = 1, 2, \cdots, N)$. Red line: nodes in H; Blue line: nodes in S; (**b**) number of disconnected components as a function of time t; (**c**) average of the correlation between pairs of oscillators. The colors are graded from blue (0) to dark red (1); (**d**) the inverse of the corresponding eigenvalues of the Laplacian matrix of L versus the rank index i

the huge community H also achieve synchronization, but the synchronous state of H is different from that of S. At this time, the synchronous state of the whole network achieves the so-called "cluster synchronization." Obviously, this regime is a particular transition to the global complete synchronization for the community network. A side benefit is that one can easily detect the community structure of a network during the stage of cluster synchronization. Finally, when the time is long enough, with $t > 30$ here, all oscillators in the whole network are entrained to the "global complete synchronization" state.

According to [24, 25], the number of zero eigenvalues of $\mathscr{D}_T(t)$ in (4.17) indicates the number of connected components of the dynamical (synchronized) network. Figure 4.19b plots the number of disconnected components as a function of time. At the beginning, all nodes are uncorrelated, so there are N disconnected sets. As

time goes on, some nodes become synchronized to each other and then merge into groups until a single synchronized component is formed after a long enough time. One can observe two plateau regions here, which indicate the relative stability of the dynamics at a given time scale. Notice that the plateau of 300 communities is shorter than the plateau of 2 communities, namely, the synchronization of 2 groups is much more stable than 300 groups, indicating that the 2-group community has better coherence in topological structure.

From Figs. 4.19b and d, one can see that there is a link between the stability of these regions and the spectrum of the Laplacian matrix. The huge gaps between eigenvalues indicates the existence of a relatively stable community structure. It can be observed that three groups of eigenvalues are separated by gaps. Each gap separates two communities, with 550, 300, or 2 groups of nodes. The synchronization dynamics and the spectrum of the Laplacian matrix, which reflects the topological structure of the network, show a surprising similarity.

Finally, Fig. 4.19c presents $\rho_{ij}(t)$ at a fixed time instant, $t = 2\,s$. At this instant, the whole network is at the stage of cluster synchronization, and it is easy to identify the separation of two communities. Therefore, the network is very close to a state in which two communities are synchronized individually, with different synchronous states from each other, once again proving the side benefit of cluster synchronization in community identification.

Similar synchronization processes can be observed for other communities, as shown in Fig. 4.20. Here, Fig. 4.20a displays the evolution of oscillators in a network consisting of two fully connected communities. There exists a clear transition to global complete synchronization. Figure 4.20b also verifies that the community structure of the two communities is very stable. In Fig. 4.20c, one can see that the network with three communities has a trend moving towards cluster synchronization. However, this transition is not as obvious as that of the community network shown in Fig. 4.20a. This is because the network in Fig. 4.20c has an inapparent community structure, where the first community is a small-world model of 100 nodes with $p = 0.01$, which has very sparse edges. Figure 4.20d shows an even fuzzier community structure of three communities, which is consistent with Fig. 4.20c.

Based on the above-described analysis, one can draw the following conclusions. (1) For community networks, there exists a general path to achieve global complete synchronization as time goes on: non-synchronization $\rightarrow$ partial synchronization $\rightarrow$ cluster synchronization $\rightarrow$ global complete synchronization. (2) Synchronization processes can be used to identify topological scales, that is, communities at different time scales. (3) Synchronization dynamics have a strong relation with the spectrum of the Laplacian matrix, which reflects the topological structure of the network.

Finally, it is remarked that this chapter only discusses complex networks of identical nodes. As to networks of non-identical nodes, spectral analysis becomes much more complicated, even for cluster synchronization (see, e.g., [51,52]), which is beyond the scope of the present study.
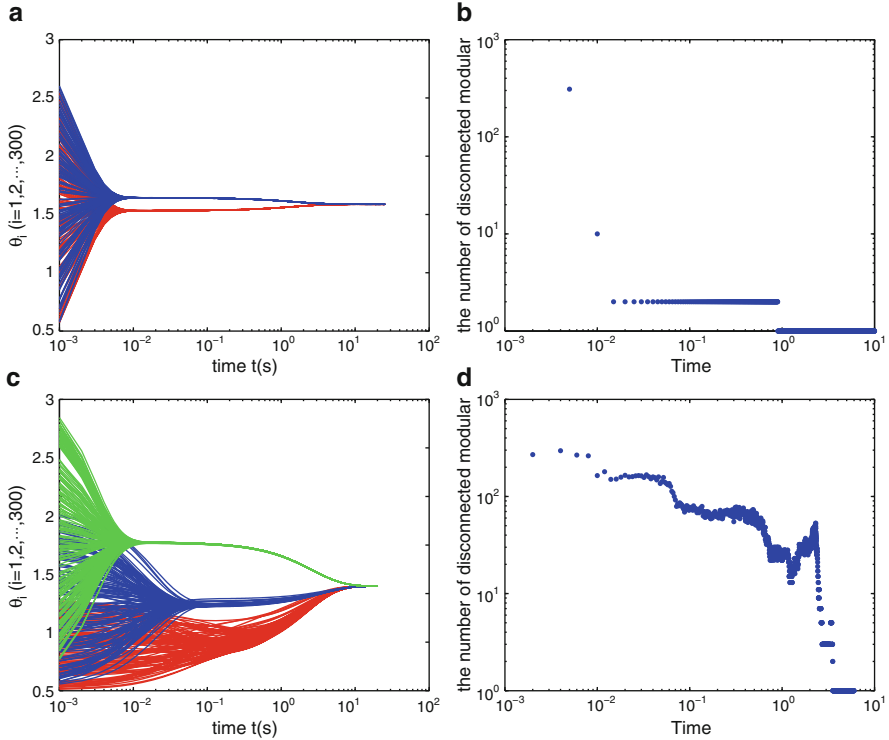
Fig. 4.20 *Top*: Network with 2 communities; each is a fully connected model of 150 nodes. There are 10 edges between the two communities. (**a**) The time evolution of oscillators θ_i $(i = 1, 2, \cdots, N)$. Red line: nodes in one community; Blue line: nodes in the other community. (**b**) Number of disconnected components as a function of time t. *Bottom*: Network with 3 communities: the first one is a small-world model of 100 nodes, with $p = 0.01$; the second is a small-world model of 150 nodes, with $p = 0.1$; the third is a small-world model of 200 nodes, with $p = 0.5$. There are 5 edges between every pair of communities. (**c**) The time evolution of oscillators θ_i $(i = 1, 2, \cdots, N)$. *Red line*: nodes in the first community; *Blue line*: nodes in the second community; *Green line*: nodes in the third community. (**d**) Number of disconnected components as a function of time t

4.6   Conclusions

The Laplacian spectra of several typical complex networks, particularly community networks, have been analyzed mainly from a numerical simulation approach. It is found that four representative complex networks have completely different spectra, where for ER random and NW small-world networks, the smallest nonzero eigenvalue λ_2 depends approximately linearly on the connection probability p. For community networks, the number of eigenvalues near zero reflects the number of communities identifiable from the network. In particular, for random, small-world, and scale-free networks, their spectra are positively correlated to their degree sequences. To find an approximated eigenvalue λ_{i+1} from λ_i, a local

prediction-correction algorithm has been proposed, which is shown to be very effective. Furthermore, paths to complete synchronization and generalized synchronization of different networks have been investigated, concluding that the synchronization processes are different with respect to different topological structures, and that nodes with the largest degree firstly achieve synchronization (and generalized synchronization) and then synchronous dynamics spread out to the rest nodes in the network. It has also been found that there is a general path towards global complete synchronization: non-synchronization → partial synchronization → cluster synchronization → global complete synchronization. Finally, it has been revealed that the gaps existing in a Laplacian spectrum are largely dependent on the stability of the communities of the networks at different time scales. All these new findings should provide useful insights to a better understanding of complex network synchronization.

References

1. Albert, R., Barabási, A.-L.: Statistical mechanics of complex networks. Reviews of Modern Physics **74**, 47–92 (2002).
2. Dorogovtsev, S.N., Mendes, J.F.F.: Evolution of Networks. Advances in physics **51**, 1079–1187 (2002).
3. Newman, M.E.J.: The structure and function of complex networks. SIAM Review **45**, 167–256 (2003).
4. Boccaletti, S., Latora, V., Moreno, Y., Chavez, M., Hwanga, D.-U.: Complex networks: Structure and dynamics. Physics Reports **424**, 175–308 (2006).
5. Newman, M.E.J.: Networks: An Introduction. Oxford University Press, UK (2010).
6. Albert, R., Jeong, H., Barabási, A.-L.: Error and attack tolerance of complex networks. Nature (London) **406**, 378–382 (2000).
7. Callaway, D.S., Newman, M.E.J., Strogatz, S.H., Watts, D.J.: Network robustness and fragility: Percolation on random graphs. Phys. Rev. Lett. **85**, 5468–5471 (2000).
8. Pastor-Satorras, R., Vespignani, A.: Epidemic spreading in scale-free networks. Phys. Rev. Lett. **86**, 3200–3203 (2001).
9. Moreno, Y., Pastor-Satorras, R., Vespignani, A.: Epidemic outbreaks in complex heterogeneous networks. Eur. Phys. J. B **26**, 521–529 (2002).
10. Nishikawa, T., Motter, A.E., Lai, Y.-C., Hoppensteadt, F.C.: Heterogeneity in oscillator networks: Are smaller worlds easier to synchronize? Phys. Rev. Lett. **91**, 014101 (2003).
11. Sorrentino, F., di Bernardo, M., Garofalo, F.: Synchronizability and synchronization dynamics of complex networks with degree-degree mixing. Int. J. Bifurcation Chaos, **17**, 2419–2434 (2007).
12. Hong, H., Kim, B.J., Choi, M.Y., Park, H.: Factors that predict better synchronizability on complex networks. Phys. Rev. E **65**, 067105 (2002).
13. Barahona, M., Pecora, L.M.: Synchronization in small-world systems. Phys. Rev. Lett. **89**, 054101 (2002).

14. Hong, H., Choi, M.Y., Kim, B.J.: Synchronization on small-world networks. Phys. Rev. E **69**, 026139 (2004).
15. Atay, F.M., Bıyıkoğlu, T., Jost, J.: Network synchronization: Spectral versus statistical properties. Physica D **224**, 35–41 (2006).
16. Chen, G., Duan, Z.: Network synchronizability analysis: A graph-theoretic approach. Chaos **18**, 037102 (2008).
17. Pecora, L.M., Carroll, T.L.: Master stability functions for synchronized coupled systems. Phys. Rev. Lett. **80**, 2109–2112 (1998).
18. Jost, J., Joy, M.P.: Spectral properties and synchronization in coupled map lattices. Phys. Rev. E **65** 016201 (2002).
19. Lü, J., Yu, X., Chen, G., Cheng, D.: Characterizing the synchronizability of small-world dynamical networks. IEEE Trans. Circuits Syst. I **51**, 787–796 (2004).
20. Nishikawa, T., Motter, A.E.: Maximum performance at minimum cost in network synchronization. Physica D **224**, 77–89 (2006).
21. Newman, M.E.J.: Finding community structure in networks using the eigenvectors of matrices. Phys. Rev. E **74**, 036104 (2006).
22. Oh, E., Rho, K., Hong, H., Kahng, B.: Modular synchronization in complex networks. Phys. Rev. E **72**, 047101 (2005).
23. Zhou, C., Kurths, J.: Hierarchical synchronization in complex networks with heterogenous degrees. Chaos **16**, 015104 (2006).
24. Arenas, A., Díaz-Guilera, A., Pérez-Vicente, C.J.: Synchronization reveals topological scales in complex network. Phys. Rev. Lett. **96**, 114102 (2006).
25. Arenas, A., Díaz-Guilera, A., Pérez-Vicente, C.J.: Synchronization processes in complex networks. Physica D **224** 27–34 (2006).
26. Gómez-Gardeñes, J., Moreno, Y., Arenas, A.: Paths to synchronization on complex networks. Phys. Rev. Lett. **98**, 034101 (2007).
27. Gómez-Gardeñes, J., Moreno, Y., Arenas, A.: Synchronizability determined by coupling strengths and topology on complex networks. Phys. Rev. E. **75**, 066106 (2007).
28. Hung, Y.C., Huang, Y.T., Ho, M.C., Hu, C.K.: Paths to globally generalized synchronization in scale-free networks. Phys. Rev. E **77**, 016202 (2008).
29. Wu, W., Chen, T.P.: Partial synchronization in linearly and symmetrically coupled ordinary differential systems. Physica D **238**, 355–364 (2009).
30. Guan, S.G., Wang, X.G., Gong, X.F., Li, K., Lai, C.H.: The development of generalized synchronization on complex networks. Chaos **19**, 013130 (2009).
31. Chen, J., Lu, J., Wu, X., Zheng, W.X.: Generalized synchronization of complex dynamical networks via impulsive control. Chaos **19**, 043119 (2009).
32. Liu, H., Chen, J., Lu, J., Cao, M.: Generalized synchronization in complex dynamical networks via adaptive couplings,. Physica A **389**, 1759–1770 (2010).
33. Mohar, B.: Graph Laplacians. In: Topics in Algebraic Graph Theory, pp. 113–136. Cambridge University Press, Cambridge (2004).
34. Atay, F.M., Bıyıkoğlu, T.: Graph operations and synchronization of complex networks. Phys. Rev. E **72**, 016217 (2005).
35. Biggs, N.: Algebraic Graph Theory. 2nd ed., Cambridge Mathematical Library, Cambridge (1993).
36. Fiedler, M.: Algebraic connectivity of graphs. Czechoslovak Mathematical Journal **23**, 298–305 (1973).
37. Anderson, W.N., Morley, T.D.: Eigenvalues of the Laplacian of a Graph. Linear and Multilinear Algebra **18**, 141–145 (1985) (Widely circulated in preprint form as University of Maryland technical report TR-71-45, October 1971).
38. Merris, R.: A note on Laplacian graph eigenvalues. Linear Algebra and its Applications **285**, 33–35 (1998).
39. Rojo, O., Sojo, R., Rojo, H.: An always nontrivial upper bound for Laplacian graph eigenvalues. Linear Algebra and its Applications **312**, 155–159 (2000).

40. Li, J., Pan, Y.: A note on the second largest eigenvalue of the Laplacian matrix of a graph. Linear and Multilinear Algebra **48**, 117–121 (2000).
41. Merris, R.: Laplacian matrices of graphs: a survey. Linear Algebra and its Applications **197/198** 143–167 (1994).
42. Duan, Z., Liu, C., Chen, G.: Network synchronizability analysis: The theory of subgraphs and complementary graphs. Physica D **237**, 1006–1012 (2008).
43. Wang, X.F., Chen, G.: Synchronization in scale-free dynamical networks: Robustness and fragility. IEEE Trans. on Circ. Syst.-I **49**, 54–62 (2002).
44. Wang, X.F., Chen, G.: Synchronization in small-world dynamical networks. Int. J. of Bifur. Chaos **12**, 187–192 (2002).
45. Erdös, P., Rényi, A.: On the evolution of random graphs. Pul. Math. inst. Hung. Acad. Sci. **5**, 17–60 (1960).
46. Newman, M.E.J., Watts, D.J.: Renormalization group analysis of the small-world network model. Phys. Lett. A **263**, 341–346 (1999).
47. Barabási, A.-L., Albert, R.: Emergence of scaling in random networks. Science **286**, 509–512 (1999).
48. Jalan, S., Bandyopadhyay, J.N.: Random matrix analysis of network Laplacians. Physica A **387**, 667–674 (2008).
49. Zhan, C., Chen, G., Yeung, L.F.: On the distributions of Laplacian eigenvalues versus node degrees in complex networks. Physica A **389** 1779–1788 (2010).
50. Acebrón, J.A., Bonilla, L.L., Pérez-Vicente, C.J., Ritort, F., Spigler, R.: The Kuramoto model: A simple paradigm for synchronization phenomena. Rev. Mod. Phys. **77**, 137–185 (2005).
51. Brede, M.: Local vs. global synchronization in networks of non-identical Kuramoto oscillators. European Phys. J. B **62** 87–94 (2008).
52. Lu, W.L., Liu, B., Chen, T.P.: Cluster synchronization in networks of coupled non-identical dynamical systems. Chaos **20** 013120 (2010).